TECHNICAL MEMORANDUMS

NATIONAL ADVISORY COMMITTEE FOR AERONAUTICS

No. 737

CONVERSION OF ENERGY IN CROSS-SECTIONAL DIVERGENCES UNDER DIFFERENT CONDITIONS OF INFLOW

By H. Peters

Ingenieur-Archiv, Vol. II, 1931

Washington
March 1934

NATIONAL ADVISORY COMMITTEE FOR AERONAUTICS

TECHNICAL MEMORANDUM NO. 737

CONVERSION OF ENERGY IN CROSS-SECTIONAL DIVERGENCES UNDER DIFFERENT CONDITIONS OF INFLOW*

By H. Peters

SUMMARY

This investigation treats of the conversion of energy in conically divergent channels with constant opening ratio and half included angle of from 2.6 to 90°, the velocity distribution in the entrance section being varied from rectangular distribution to fully developed turbulence by changing the length of the approach. The energy conversion is not completed in the exit section of the diffuser; complete conversion requires a discharge length which depends upon the included angle and the velocity distribution in the entrance section. For that reason the efficiency (ratio of rise of pressure energy to difference of kinetic energy of mean velocity) was determined, once for the diffuser alone, then with the discharge length necessary for complete conversion. These efficiencies are, in part, widely at variance, and it was found that the velocity distribution in the entrance section affects the pressure conversion very profoundly in the diffuser, alone,* but only very little in the diffuser with exit length. A comparison with Gibson's experiments at a greater opening ratio, concedes the efficiency to be dependent on this ratio, especially for large included angles. Complete elucidation of this interdependence awaits further investigations as comparative quantities. The conversion losses proportionate to the losses by sudden divergence (Carnot loss) are preferable to the efficiency.

In order to compare diffusers with different energy distributions, we assume as efficiency of the diffuser with entrance length, the ratio of actual rise of energy

---

*"Energieumsetzung in Querschnittserweiterungen bei verschiedenen Zulaufbedingungen." Ingenieur-Archiv, vol. II, 1931, pp. 92-107.

to the difference of the mean kinetic energies (not the kinetic energy of the mean velocities). In the extreme case of developed turbulent profile in the entrance section, the discrepancy of the so defined efficiency was 5 percent relative to the first.

Lastly, a spiral fan was mounted in the extreme length and the effect of the spiral flow on the energy conversion in the cross-sectional divergence explored. The spiral flow was measured so that the efficiency could be unequivocally defined. A comparison with the efficiency in pure axial flow reveals a marked increase as the spiral becomes more intense.

INTRODUCTION

The results of previous experiments on circular, conically divergent channels, assume a particular significance within the scope of the present paper. Figure 1 is an attempt to illustrate the results of Andres (reference 1), of Francis (reference 2), Banninger (reference 3), and Riffart (reference 4) in form of an efficiency η_0 versus half the included angle ϑ:

$$\eta_0 = \frac{p_2 - p_1 + p_r}{\frac{\rho}{2}(\bar{w}_1^2 - \bar{w}_2^2)}$$

wherein p = static pressure, $\bar{w}$ = mean velocity in cross section, ρ = density, subscripts 1 and 2 the respectively narrow and wide cross section, and p_r = loss due to wall friction. These data constitute partial results of quite elaborate experiments that were to yield the optimum diffuser form. Contributory factors such as ratio of orifice, roughness, attitude of flow in entrance section, etc., which influence the conversion of energy, were not sufficiently separated from one another or else not accurately enough defined to afford conclusive evidence of the individual factors of influence. Consequently, the only legitimate method of representing these data on conical diffusers is as function of the included angle.

Whereas the principle of the experimental arrangements of the results shown in figure 1 is the same, the form and size of the chosen constrictions are different.

The different types of transition change the velocity profile in the narrowest cross section. Andres' experiments of changing this profile by installing screens, perforated disks, etc., disclosed its considerable influence. Riffart arrived at the same result. He fitted the diffuser, without previous constriction, directly to a long, straight pipe, and was, as a result, unable to obtain constant velocity across the whole section. His attempt ended in a decided impairment of efficiency. Thus the marked scattering of the data in figure 1 is not at all surprising, and especially when reflecting that the pressure taps for p_2 are not uniformly distributed across the exit section of the diffuser. Gibson's (reference 5) measurements disclose the pressure change in the exit section to be still incomplete; that rather a complete pressure conversion requires a discharge length of from 2 to 6 times the diameter. These experiments by Gibson are, by the way, the only ones in which only one influencing quantity - the included angle - was systematically changed. The results are elsewhere compared with the present experiments.

PROBLEM

By systematic variation of the velocity profile before the divergence, its influence on the energy transformation is explored. The profile was varied by changing the entrance length l (see fig. 2), and thereby from rectangular (potential flow) to fully developed turbulent velocity profile. A second problem was the examination of the influence of spiral flow - a rotation superposed on the axial flow - on the energy conversion in cross-sectional enlargements. The spiral flow was very accurately defined from the velocity components and the pressure distribution across the section.

This problem of spiral flow is of practical interest for the design of turbine suction pipes. Quite frequently the flow emerging from the runner still manifests spirals whose intensity varies with the degree of loading. Andres already attempted to explain the spiral effect and recorded increased efficiency. But his results are uncertain since he failed to give any exact definition of the spiral flow or of the recorded pressure.

The present experiments were made with pipes of circular section with straight conical divergences in air for

constant volume of flow. The included angle 2ϑ with constant cross-sectional ratio F_1/F_2 was varied between $\vartheta = 2.6°$ and $\vartheta = 90°$.

EXPERIMENTAL SET-UP (fig. 2)

It consisted primarily of seamless drawn brass tubes. The nozzle-shaped transition with steady but not undue flare from fan connection to entrance length, 6.25 contraction ratio, insured an almost rectangular velocity distribution at the mouth of the entrance length. The spiral freedom, which stipulates constant static pressure across the section, was checked by ststic pressure survey. In order to insure an extensive variation of entrance length, the latter was built up of sections of varying length. By centering the flange (fig. 3) an almost shock-free transition from one length to the other was obtained, according to the pressure records taken along the pipe section. The structural details of the conical pipe section are shown in figure 3. To assure that the surface of the diffuser, which was made of plaster, was similar to that of the brass tube, it was coated with shellac and polished. The V.D.I. standard nozzle No. 1912 in the return passage of 175 mm diameter served to define the mean rate of flow.

The static pressure along the test section was surveyed through four 0.8 mm* holes each in every test section with annular compensating chamber (fig. 4). The velocity distribution across a section was determined from the static pressure and the total pressure record as shown in figure 4.

The spiral flow was produced by a guide apparatus (fan) (fig. 5) mounted between the entrance length and the transition piece from the fan connection. The aim was a spiral flow with constant angular velocity as with a rigid body. The flow direction is given with $\tan \delta = u/w$, wherein u = tangential component, and w = axial component of velocity. The basis of calculation for the guide apparatus is briefly as follows: If the axial component w of the flow velocity c is constant across the section, the angular velocity is:

$$\Omega = \frac{u_R}{R} = \frac{1}{R} w \tan \delta_R$$

*mm × .03937 = in.

and the tangential component u of velocity c becomes

$$u = \frac{r}{R} w \tan \delta_R;$$

wherein r = arbitrary radius, R = pipe radius, u_R = tangential velocity at wall, and δ_R = angle of flow direction at the wall. The spiral momentum

$$d J = 2 \pi \rho \frac{r^2}{R} w^2 \tan \delta_R \, r \, dr$$

must equal the moment of the lift of the blades

$$r \, d A = \frac{\rho}{2} w^2 c_a \, z \, t \, r \, dr.$$

Hence,

$$t \, z \, c_a = 4 \pi \frac{r^2}{R} \tan \delta_R,$$

with t = blade chord, z = number of blades, and c_a = coefficient of lift of blade profile. Constant axial velocities w behind the guide apparatus are obtained by decelerating the inner stream filaments through protuberances, since the absolute velocity c and the pressure p are greater toward the wall than in the center.

Example: The value $\frac{u}{w} = \tan \delta_R = 1$ is desired on the wall of the pipe with radius $R = 0.035$ m. The choice is $z = 12$, $t_R = 0.04$ m,* then $c_a = 1.1$. Now the selection of a circular arc profile with $\frac{f}{t} = 0.1$ blade curvature, reveals the angle of attack α of the profile at $\alpha = 3.5^\circ$ with a $1/\infty$ aspect ratio. Since the tangential velocity at the blade itself is half as great as behind the blade, the actual direction of flow β is

$$\tan \beta = \frac{u}{2 w} = \tfrac{1}{2} \tan \delta_R.$$

The angle of the blade profile to the axis of flow is disclosed at $(\alpha + \beta) = 30^\circ$. (See fig. 6.)

A more exact determination of the spiral flow before the diffuser requires the measurement of flow direction, total pressure, and static pressure at the wall. A suitable instrument is a cylindrical tube of 2 mm diameter with an 0.3 mm hole on the side. The set-up was similar to that of figure 4 but fitted with a device permitting the turning

*m × 39.37 = in.

of the cylindrical tube. Owing to the inaccuracy of the zero method, i.e., turning of instrument up to maximum pressure reading, two symmetrical points of the curve $p = f(\delta')$ were established by pressure comparison in the zone of the higher pressure gradient, and the slope δ of the flow direction toward the tube axis defined therefrom. The total pressure was recorded with the same instrument by turning it into the direction of flow, and the static pressure through pressure taps in the wall, as before. The static pressure on the inside was arrived at mathematically because of the experimental difficulties involved.

DEFINITION OF EFFICIENCY

The conventional, elementary equation for defining the efficiency

$$\eta = \frac{p_2 - p_1}{\frac{\rho}{2} \bar{w}_1^2 + \frac{\rho}{2} \bar{w}_2^2} = \frac{p_2 - p_1}{\frac{\rho}{2} \bar{w}_1^2 \left[1 - \left(\frac{F_1}{F_2} \right)^2 \right]} \tag{1}$$

fails in the comparison of conversion of energy with arbitrary distribution of kinetic energy across the section.

According to the law of energy, we have with the absolute velocity c

$$\int^{F_1} \left(p_1 + \frac{\rho}{2} c_1^2 \right) w_1 \, dF - \int^{F_2} \left(p_2 + \frac{\rho}{2} c_2^2 \right) w_2 \, dF - E_v = 0, \tag{2}$$

disregarding the time rate of change in velocity if E_v is the power loss. Thus, beginning with the purpose of the diffuser, to change kinetic into potential energy, the efficiency is the ratio of the actual rise in pressure energy to the difference in kinetic energies

$$\eta_{total} = \frac{\int^{F_2} p_2 \, w_2 \, dF - \int^{F_1} p_1 \, w_1 \, dF}{\int^{F_1} \frac{\rho}{2} c_1^2 \, w_1 \, dF - \int^{F_2} \frac{\rho}{2} c_2^2 \, w_2 \, dF} =$$

$$1 - \frac{E_v}{\int^{F_1} \frac{\rho}{2} c_1^2 \, w_1 \, dF - \int^{F_2} \frac{\rho}{2} c_2^2 \, w_2 \, dF} \tag{3}$$

The representative trend of the pressure at the wall, illustrated in figure 7, proves that the pressure conversion is not completed in the exit section of the diffuser, that there is rather a further rise of pressure in the discharge channel. As a result, two efficiencies can be deduced, namely:

η_I for the diffuser alone (p_{2_I} in exit section),

η_{II} for the diffuser with the discharge channel ($p_{2_{II}}$ in section of maximum pressure).

We first treat the case of pure axial flow, for which $u = 0$ and consequently $c = w$ and pressure p = constant across the section. Then equation (3) becomes

$$\eta_{total} = \frac{(p_2 - p_1)\ \bar{w}_1\ F_1}{\int_{F_1} \frac{\rho}{2} w_1^3\ dF - \int_{F_2} \frac{\rho}{2} w_2^3\ dF} \tag{4}$$

or, with

$$\int_{F_1} \frac{\rho}{2} w_1^3\ dF = A\ \frac{\rho}{2} \bar{w}_1^3\ F_1 \quad \text{and} \quad \int_{F_2} \frac{\rho}{2} w_2^3\ dF = B\ \frac{\rho}{2} \bar{w}_2^3\ F_2$$

$$\eta_{total} = \frac{p_2 - p_1}{\frac{\rho}{2} \bar{w}_1^2\ A - \frac{\rho}{2} \bar{w}_2^2\ B} = \frac{p_2 - p_1}{\frac{\rho}{2} \bar{w}_1^2 \left[A - B \left(\frac{F_1}{F_2}\right)^2\right]} \tag{4a}$$

The definition of the efficiency solely on the basis of mean velocity $\bar{w}$, yields an efficiency in accord with equation (1) whose connection with η_{total} is given in

$$\eta = \frac{p_2 - p_1}{\frac{\rho}{2} \bar{w}_1^2 \left[1 - \left(\frac{F_1}{F_2}\right)^2\right]} = \eta_{total} \frac{A - B \left(\frac{F_1}{F_2}\right)^2}{1 - \left(\frac{F_1}{F_2}\right)^2} \tag{5}$$

For nearly rectangular velocity distributions, i.e., $w = \bar{w}$, A becomes $= B \approx 1$ and therefore, $\eta = \eta_{total}$. Outside of the rectangular distribution of velocity the developed turbulent distribution produced with sufficiently

long entrance length, is more readily amenable to calculation, and is therefore given here.

Prandtl's theorem (reference 6), according to which the velocities at a Reynolds Number of $R = 2 \times 10^5$ are proportionate to the 1/7 power of the wall distance, discloses for the turbulent velocity distribution

$$\frac{w}{w_{max}} = \left(1 - \frac{r}{R}\right)^{1/7},$$

w_{max} being the velocity in the axis of the pipe. Then the mean velocity is

$$\frac{\overline{w}}{w_{max}} = 0.816,$$

and the relation of the actual flow of kinetic energy per second to the flow energy per second of the mean velocity is:

$$A = \frac{1}{F} \int \left(\frac{w}{\overline{w}}\right)^3 dF = 1.06.$$

A better approximation* to the test data is obtained by rounding off the velocity distribution in the channel center with

$$\frac{w}{w_{max}} = \left[1 - \left(\frac{r}{R}\right)^m\right]^{1/7}$$

This equation gives for $m = 2$,

$$\frac{\overline{w}}{w_{max}} = 0.875 \quad \text{and} \quad A = 1.045.$$

*The only attempt to analyze this conversion loss mathematically was, as far as I know, made by H. Lorenz, in the Stodola Jubilee paper, and published in Zeitschrift für Technische Physik, vol. 10, 1929, p. 303. Although the physical argumentation of his theorem does not seem unconditionally cogent, the final result $p_u = \frac{\rho}{2}(\overline{w}_1^2 - \overline{w}_2^2) \frac{4}{3} \tan \vartheta$ with divergent angles up to $\vartheta = 10^\circ$ depicts the results for smooth pipes very well.

As regards the velocity distribution in the discharge channel and consequently of B, no summary predictions can be made. But one result of the present investigation, is that the velocity distribution in the section of maximum pressure of the discharge channel is somewhat more complete than the developed turbulent velocity distribution and practically independent of the angle of divergence and of the distribution in inflow section. The evaluation gave

$$B = \frac{1}{F_2} \int \left(\frac{w_2}{\bar{w}_2}\right)^3 dF = 1.025 \text{ to } 1.035$$

Figuring with a mean $B = 1.03$ for turbulent velocity distribution in the inflow section, and with $\frac{w}{w_{max}} = \left[1 - \left(\frac{r}{R}\right)^2\right]^{1/7}$ and $\frac{F_1}{F_2} = 0.427$ cross-section ratio, we obtain

$$\frac{\eta}{\eta_{total}} = 1.05.$$

The pressure losses p_v, computable from equations (3) and (5) as

$$\frac{p_v}{\frac{\rho}{2}\left(\bar{w}_1^2 - \bar{w}_2^2\right)} = \frac{A - B\left(\frac{F_1}{F_2}\right)^2}{1 - \left(\frac{F_1}{F_2}\right)^2} - \eta,$$

can be divided into wall friction losses p_r and conversion losses p_u.* The former can be defined like the losses in a straight pipe as

$$p_r = \int \lambda \frac{\rho}{2} (\bar{w})^2 \frac{dl}{r} \qquad (6)$$

λ being the coefficient of pipe friction. For the diffuser with constant angle 2ϑ, we then obtain - assuming λ = constant -

$$\frac{p_r'}{\frac{\rho}{2}\bar{w}_1^2 - \frac{\rho}{2}\bar{w}_2^2} = \frac{\lambda}{4 \tan \vartheta}$$

and, for the discharge channel of length l_a up to the

*See footnote, page 8.

section of maximum pressure,

$$\frac{p_r''}{\frac{\rho}{2}\bar{w}_1^2 - \frac{\rho}{2}\bar{w}_2^2} = \frac{\lambda}{\left(\frac{F_2}{F_1}\right)^2 - 1}\,\frac{l_a}{R_2}$$

Taking cognizance of these frictional losses, it yields

$$\eta_{O_I} = \eta_I + \frac{\lambda}{4\tan\vartheta} = \frac{(p_2 - p_1)_I}{\frac{\rho}{2}\bar{w}_1^2\left[1 - \left(\frac{F_1}{F_2}\right)^2\right]} + \frac{\lambda}{4\tan\vartheta} \qquad (7)$$

for the diffuser alone, and

$$\eta_{O_{II}} = \eta_{II} + \frac{\lambda}{4\tan\vartheta} + \frac{\lambda}{\left(\frac{F_2}{F_1}\right)^2 - 1}\,\frac{l_a}{R_2} = \frac{(p_2 - p_1)_{II}}{\frac{\rho}{2}\bar{w}_1^2\left[1 - \left(\frac{F_1}{F_2}\right)^2\right]} +$$

$$+ \frac{\lambda}{4\tan\vartheta} + \frac{\lambda}{\left(\frac{F_2}{F_1}\right)^2 - 1}\,\frac{l_a}{R_2}$$

for the diffuser with discharge channel.

For spiral flow, equation (3) gives

$$\eta_{total} = \frac{\int_{F_1}^{F_2} p_2\, w_2\, dF - \int_{F_1}^{F_2} p_1\, w_1\, dF}{\int_{F_1}^{F_2} \frac{\rho}{2} c_1^2\, w_1\, dF - \int_{F_1}^{F_2} \frac{\rho}{2} c_2^2\, w_2\, dF},$$

wherein $c^2 = u^2 + w^2$ and $p = p_{(r=\rho)} + \int_{\rho}^{r} \rho\, u^2\, \frac{dr}{r}$.

For the special case of rigid spiral ω = constant and $w = \bar{w}$ = constant, and efficiency can be deduced whose factors lend themselves more readily to measurement. The energy is computed as

$$E = \int^{F} \left[p_{(r=o)} + \rho\,\omega^2\, r^2 + \frac{\rho}{2}\bar{w}^2\right] \bar{w}\, dF$$

$$= \left[p_{(r=o)} + \frac{\rho}{2}\omega^2 R^2 + \frac{\rho}{2}\bar{w}^2\right] \bar{w}\, F = \left[p_R + \frac{\rho}{2}\bar{w}^2\right] \bar{w}\, F.$$

so that the energy equation (2) can be written

$$p_{R_1} + \frac{\rho}{2} \bar{w}_1^2 - p_{R_2} - \frac{\rho}{2} \bar{w}_2^2 - p_v = 0$$

and finally, the efficiency

$$\eta = \frac{p_{R_2} - p_{R_1}}{\frac{\rho}{2} (\bar{w}_1^2 - \bar{w}_2^2)} \qquad (8)$$

Obviously the thus-defined efficiency is valid only for this assumed spiral distribution and inapplicable to other distributions.

EXPERIMENTS AND INTERPRETATION

All measurements were made with approximately the same volume of flow, as stated at the beginning. The volume was defined at

$$Q = \alpha F \sqrt{\frac{2}{\rho} \Delta p};$$

Δp = pressure gradient at standard nozzle of 175 mm diameter in the return passage. Since the narrowest section F of the entrance length happened to equal section F_1 of the entrance length, the dynamic pressure of the mean velocity in section F_1 is

$$\frac{\rho}{2} \bar{w}_1^2 = \alpha^2 \Delta p.$$

The coefficient of flow α was taken at $\alpha = 0.97$ from a report by Mueller and Peters (reference 7). This dynamic pressure was kept constant for all measurements: $\frac{\rho}{2} \bar{w}^2 = 112$, which gave as Reynolds Number for a mean kinematic viscosity ν

$$R = \frac{w D_1}{\nu} = 2 \times 10^5.$$

a) Preliminary surveys.- In order to avoid flow disturbances before the diffuser during surveys with pitot tubes, etc., the measurements of the velocity distribution

and of the spiral flow were made separately for different entrance lengths.

Figure 8 shows the velocity distributions $\frac{w}{w_{max}} = f\left(\frac{r_1}{R_1}\right)$ recorded in pure axial flow without diffuser. The profile was symmetrical to the axis of the pipe. The instrumental accuracy was checked with the continuity equation

$$\int_{F_1} w_1 \, dF = \bar{w}_1 \, F_1 .$$

The mean velocity arrived at by integration was, on the whole, 1 percent higher than that obtained with the standard nozzle. Indisputable proof of the cause of this discrepancy was not obtained. It might be due to erroneous measurement of the static pressure through the wall orifices,* or it might have been caused by erroneous measurement of the total pressure adjacent to the wall. Another source of error is the inevitable velocity fluctuation, since the pitot tube records the mean value of w^2 with respect to time and is consequently always greater than $(w_{mean})^2$.

From the velocity distribution we deduced the value A, which compares the flow of kinetic energy per second with the product of flow volume $\bar{w}_1 \, F_1$ and the kinetic energy of mean velocity $\frac{\rho}{2} (\bar{w}_1)^2$:

$$A = \frac{1}{F_1} \int_{F_1} \left(\frac{w_1}{\bar{w}_1}\right)^3 dF.$$

In figure 9, A is plotted against entrance length l/D_1. It also shows the pressure drop in this length. The wall pressure p relative to dynamic pressure $\frac{\rho}{2} (\bar{w}_1)^2$ is shown versus the entrance length.

The coefficient of pipe friction λ between $l = 50$ and 60 D_1 is:

$$\lambda = \frac{p_r}{\frac{\rho}{2} \bar{w}_1^2} \frac{R_1}{\Delta l} = 0.0083$$

*In G. Fuhrmann's "Theoretische und experimentelle Untersuchungen an Ballonmodellen," Berlin, 1912, the measurements were made with an 0.8 mm orifice diameter and gave static pressures approximately 0.8 percent too low.

This figure agrees with that of Stanton and Pannell (reference 8), that is, $\lambda = 0.008$, fairly closely for equal Reynolds Number.

For spiral flow we determined the flow direction in the different sections by the angle of flow direction δ with the pipe axis and the total pressure p_g and measured the wall pressure p_R. Figure 10 shows the values

$$\tan \delta = \frac{u}{w} = f\left(\frac{r_1}{R_1}\right)$$

for the individual sections. The lack of symmetry with the pipe axis is due to inaccuracies in workmanship of the guide apparatus, and partly due also to a slight curvature of the test section as disclosed in subsequent experiments.

The static pressure on the inside yielded to step-by-step integration

$$p = p_R + \int_R^r \rho\, u^2 \frac{dr}{r} = p_R + 2 \int_R^r \sin^2 \delta\, (p_g - p) \frac{dr}{r}.$$

Figures 11-16 give velocity components $u_1/\overline{w}_1$ and $w_1/\overline{w}_1$ versus r_1/R_1. The values obtained across a diameter are plotted with different notation of the test points against a radius. The solid dots refer to one, the rings to the other half of the test diameter.

The instrumental accuracy, again checked by comparing the integration result with that from the standard nozzle, ranged within -1 percent and +2 percent.

The flow of energy per second through each section with spiral flow, was determined as for axial flow and equated to the flow energy per second of the mean velocity. These equations are:

$$\frac{1}{F_1} \int^{F_1} \left(\frac{c_1}{\overline{w}_1}\right)^2 \frac{w_1}{\overline{w}_1}\, dF, \quad \text{for the kinetic energy,}$$

$$\frac{1}{F_1} \int^{F_1} \left(\frac{u_1}{\overline{w}_1}\right)^2 \frac{w_1}{\overline{w}_1}\, dF, \quad \text{for the spiral energy,}$$

$$\frac{1}{F_1}\int^{F_1}\frac{p_1}{\frac{\rho}{2}\bar{w}_1^2}\frac{w_1}{\bar{w}_1}\,dF, \quad \text{for the pressure energy,}$$

$$\frac{1}{F_1}\int^{F_1}\frac{p_g}{\frac{\rho}{2}\bar{w}_1^2}\frac{w_1}{\bar{w}_1}\,dF, \quad \text{for the total energy.}$$

They are given in figure 17 versus entrance length l/D_1. The plot also shows the pressure $\frac{p_R}{\frac{\rho}{2}\bar{w}_1^2}$ at the pipe wall and the pressure $\frac{p(r=o)}{\frac{\rho}{2}\bar{w}_1^2}$ in the pipe axis.

b) The actual diffuser tests.- They revealed the pressure along the test section through holes in the walls, a case in point being shown in figure 18. From these diagrams the pressure p_1 in the entrance section is obtained by extrapolation of the pressure curve in the entrance length, the pressure $p_{2\,I}$ in the exit section by extrapolation of the pressure curve in the discharge channel up to the discharge section of the diffuser and pressure $p_{2\,II}$ as maximum pressure in the discharge channel. (Compare fig. 17.)

We start with an analysis of the investigation for pure axial flow. To define the efficiency according to (4a)

$$\eta_{total} = \frac{p_2 - p_1}{\frac{\rho}{2}\bar{w}_1^2\left[A - B\left(\frac{F_1}{F_2}\right)^2\right]},$$

the quantities $\frac{p_2 - p_1}{\frac{\rho}{2}\bar{w}_1^2}$ are taken conformably to figure 18, and $A = \frac{1}{F_1}\int^{F_1}\left(\frac{w_1}{\bar{w}_1}\right)^3 dF$ conformably to A as function of the entrance length (fig. 9). The value $B = \frac{1}{F_2}\int^{F_2}\left(\frac{w_2}{\bar{w}_2}\right)^3 dF$, which corresponds to the flow of kinetic energy per second in section F_2, must be defined from

the velocity distribution survey in section F_2, which, however, is very difficult unless the flow is orderly. As criterion for orderly flow, the start of the linear pressure drop along the section can be taken, which approximately lies in the section of maximum pressure. The distance l_a of this section from that of the diffuser exit, is contingent upon the angle of divergence and on the velocity profile in the entrance section. The possible influence of the opening ratio could not be explained by the present program which was confined to one ratio only. Figure 19 exhibits the requisite discharge lengths up to the section of maximum pressure l_a/D_2 as function of entrance length l/D_1, with the parameter of half included angle ϑ as a compensated set of curves. The accuracy is to within 0.5 to 1 D_2.

The experimental set-up permitted the measurement of the velocity distribution at 1.1 D_2, 2.9 D_2, 4.7 D_2 and 6.6 D_2 distance from the exit section of the diffuser. In these sections the velocity distribution was explored for the diffusers with $\vartheta = 3.9^\circ$, 7.35°, 14.2°, and 33.5° with 2.1 D_1, 10.1 D_1, and 27.1 D_1 entrance lengths. The evaluation revealed for the section of maximum pressure a somewhat more complete velocity profile than the developed turbulent profile, almost independent of the angle of divergence and of the velocity profile in the entrance section of the diffuser. To check the instrumental accuracy, the integrated mean velocity was compared with the velocity obtained from that of the volume. In the almost orderly flow of maximum pressure the error, always positive, amounted to +2 percent, and in the unordered flow, up to +6 percent. Value B, corresponding to the flow of energy per second in the section of maximum pressure ranged between

$$B = \frac{1}{F_2} \int^{F_2} \left(\frac{w_2}{\bar{w}_2}\right)^3 dF = 1.025 \text{ to } 1.035$$

Since the instrumental accuracy was generally not greater than ± 1 percent, the efficiency

$$\eta_{total} = \frac{(p_2 - p_a)_{II}}{\frac{\rho}{2} \bar{w}_1^2 \left[A - B \left(\frac{F_1}{F_2}\right)^2\right]}$$

was defined with a mean $B = 1.03$ for all included angles ϑ. (See fig. 20.)

Because of the inaccurate measurement in the exit section itself, the determination of β for this section was omitted and the efficiency simply defined according to (5):

$$\eta_I = \frac{(p_2 - p_1)_I}{\frac{\rho}{2}(\bar{w}_1^2 - \bar{w}_2^2)}$$

and according to (7)

$$\eta_{O_I} = \eta_I + \frac{\lambda}{4 \tan \vartheta}$$

(figs. 21 and 22). For comparison the similarly defined efficiencies of diffuser with discharge channel

$$\eta_{II} = \frac{(p_2 - p_1)_{II}}{\frac{\rho}{2}\bar{w}_1^2 - \frac{\rho}{2}\bar{w}_2^2}$$

and

$$\eta_{O_{II}} = \eta_{II} + \frac{\lambda}{4 \tan \vartheta} + \frac{\lambda}{\left(\frac{F_2}{F_1}\right)^2 - 1} \frac{l_a}{R_2}$$

are used (fig. 23) to illustrate the energy that is lost in the absence of the discharge channel. Figure 24 shows η_{O_I} as function of half included angle ϑ for different entrance lengths. Gibson's experiments, cited at the beginning of this article, were made with $2D_1$ entrance length and $\frac{F_2}{F_1} = 4.0$ ratio, and are included in figure 25. The comparison clearly shows that the efficiency even with small angles ϑ is not, as frequently assumed, independent of F_2/F_1, although the efficiency is not quite suitable for the comparison of diffusers of different F_2/F_1. It is better to use the specific conversion loss p_u as comparative quantity and to refer it to the loss at the sudden sectional divergence $\vartheta = 90^\circ$. The loss at $\vartheta = 90^\circ$ (Carnot's loss) is, according to the momentum theory

$$p_{u(\vartheta=90^\circ)} = \frac{\rho}{2}(\bar{w}_1 - \bar{w}_2)^2 = \frac{\rho}{2}\bar{w}_1^2 \left[1 - \left(\frac{F_1}{F_2}\right)\right]^2,$$

so long as the thereby stipulated assumption of constant pressure across the particular sections holds true. In the present comparative case it gives

$$\frac{p_u}{\frac{\rho}{2}(\bar{w}_1 - \bar{w}_2)^2} = (1 - \eta_{0\,II}) \frac{1 - \left(\frac{F_1}{F_2}\right)^2}{\left(1 - \frac{F_1}{F_2}\right)^2}$$

because $A - B\left(\frac{F_1}{F_2}\right)^2 \approx 1 - \left(\frac{F_1}{F_2}\right)^2$ with entrance length $\frac{l}{D_1} = 2$. Figure 26 shows $\frac{p_u}{\frac{\rho}{2}(\bar{w}_1 - \bar{w}_2)^2}$ plotted against $\frac{1}{2}\vartheta$ for $\frac{F_2}{F_1} = 2.34$ and $\frac{F_2}{F_1} = 4.0$ ratio. Here the accord of the two tests is much better; for $\vartheta = 90^\circ$ the curves approach the theoretical value 1 very closely.

The diffuser tests with spiral flow included three different spacings of the diffuser from the spiral fan - 27.1 D_1, 41.1 D_1, and 60.1 D_1 - that is, three different spiral forms. The interpolation of figure 10 yielded the spiral distribution $\tan \delta = \frac{u_1}{w_1}$ (fig. 27) for these three entrance lengths. The wall pressure p_R was recorded through taps along the test section, and the total pressure and the direction of flow defined in a section F_2 at 2.9 D_2 distance from the exit section of the diffuser. Step-by-step integration of the pressure

$$p_2 = p_{R_2} + \int_{R_2}^{r} \rho\, u_2^2 \frac{dr}{r}$$

then conceded

$$\int^{F_2} p_2\, w_2\, dF \quad \text{as well as} \quad \int^{F_2} \frac{\rho}{2} c_2^2\, w_2\, dF.$$

The potential energy in the entrance section

$$\int^{F_1} p_1\, w_1\, dF = p_{R_1}\, \bar{w}_1\, F_1 - \int^{F_1} w_1 \left(\int_0^{R_1} \rho\, u^2 \frac{dr}{r} - \int_0^{r} \rho\, u^2 \frac{dr}{r} \right) dF$$

can be determined from the pressure record p_{R_1} at the wall and the dimensionless

$$\frac{p_F}{\frac{\rho}{2}\overline{w}_1^2}, \quad \frac{p_{(r=o)}}{\frac{\rho}{2}\overline{w}_1^2} \quad \text{and} \quad \frac{1}{F_1}\int^{F_1} \frac{p}{\frac{\rho}{2}\overline{w}_1^2}\,\frac{w_1}{\overline{w}_1}\,dF$$

of figure 17. The kinetic energy in entrance section $\frac{\rho}{2}\int^{F_1} c_1^2\, w_1\, dF$ is attainable forthwith from $\frac{1}{F_1}\int^{F_1}\left(\frac{c_1}{\overline{w}_1}\right)^2 \frac{w_1}{\overline{w}_1}\,dF$ of figure 17 by multiplication with $\overline{w}_1\, F_1\, \frac{\rho}{2}\overline{w}_1^2$. The efficiencies computed from these values in accordance with (3)

$$\eta_{total} = \frac{\int^{F_2} p_2\, w_2\, dF - \int^{F_1} p_1\, w_1\, dF}{\int^{F_1} \frac{\rho}{2} c_1^2\, w_1\, dF - \frac{\rho}{2}\int^{F_2} c_2^2\, w_2\, dF}$$

are shown for 27.1 D_1, 41.1 D_1, and 60.1 D_1 diffuser spacing versus $\frac{1}{2}\vartheta$ in figure 28 along with the total efficiencies (equation (4))

$$\eta_{total} = \frac{(p_2 - p_1)_{II}\, \overline{w}_1\, F_1}{\frac{\rho}{2}\int^{F_1} w_1^3\, dF - \frac{\rho}{2}\int^{F_2} w_2^3\, dF}$$

for irrotational flow with $2D_1$ entrance length. These efficiencies are valid only for the diffuser fitted with entrance length. The determination of other efficiencies, say, according to equation (8), wherein only the wall pressure and F_2/F_1 are evaluated, was omitted, because the conditions ω = constant and $w = \overline{w}$ could in no case be exactly complied with. The efficiency for the diffuser alone was also omitted because the measurement of the velocity distribution and of the flow direction directly in the exit section involves great obstacles and even the extrapolation of the wall pressure up to the exit section engenders greater inaccuracy as a result of the marked pressure gradient, especially with large ϑ.

The distance l_a/D_2 of the section of maximum pressure from the discharge section of the diffuser is shown

in figure 29 plotted against $\frac{1}{2}\vartheta$ for the three explored spiral flows.

Translation by J. Vanier,
National Advisory Committee
for Aeronautics.

REFERENCES

1. Andres, K.: Versuche über die Umsetzung von Wassergeschwindigkeit in Druck. Mitteilungen über Forschungsarbeiten. V.D.I. (1909), p. 76.

2. Francis: Lowell Hydr. Exper. 1883.

3. Banninger: ZS f.d. ges. Turbinenwesen 3 (1906), p. 12.

4. Riffart, A.: Über Versuche mit Verdichtungsdüsen. Mitteilungen über Forschungsarbeiten. V.D.I. (1922), p. 257.

5. Gibson, A. H.: Proc. of Roy. Soc., London A 83 (1910), p. 366.

6. Karman, Th. v.: ZS f. ang. Math. u. Mech. 1 (1921), p. 233.

Nikuradse, J.: Über turbulente Wasserströmungen in geraden Rohren bei sehr grossen Reynoldsschen Zahlen; Vorträge aus dem Gebiete der Aerodynamik und verwandter Gebiete (Aachen 1929), Berlin 1930.

7. Mueller, H., and Peters, H.: Coefficients of Flow of Standard Nozzles. T.M. No. 549, N.A.C.A., 1930.

8. Stanton, T. E., and Pannell: Phil. Trans. 214 (1914), p. 199.

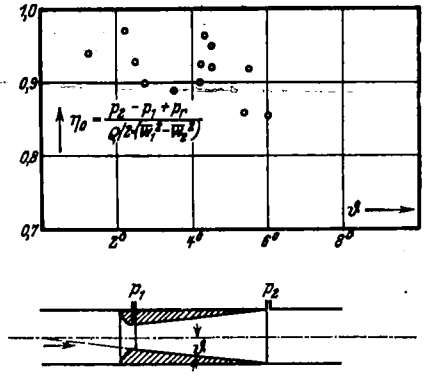

Figure 1. - Tabulation of previous experiments.

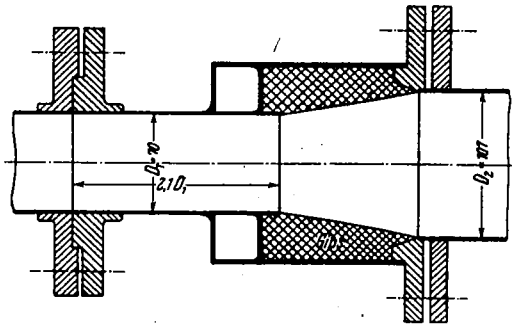

Figure 3. - The conical pipe

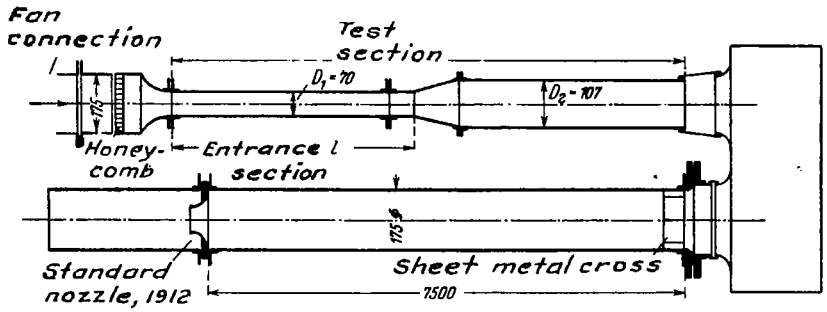

Figure 2. - Experimental set up

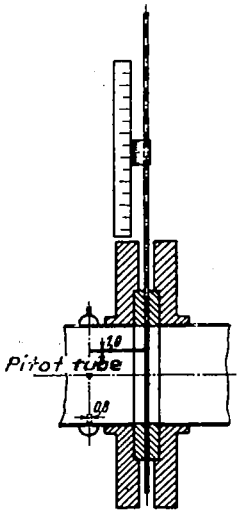

Figure 4. - Set up for pressure and velocity surveys.

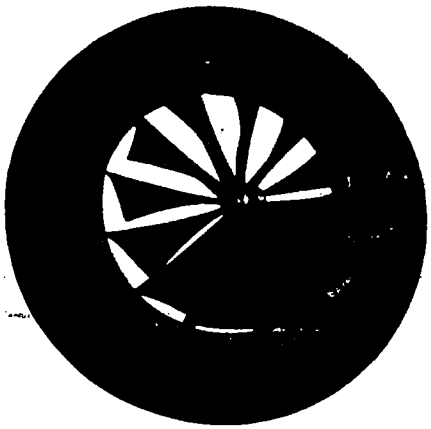

Figure 5. - Spiral fan

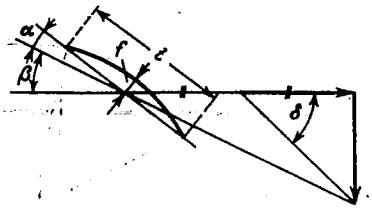

Figure 6. - Angle of attack of blade profile to axis of flow.

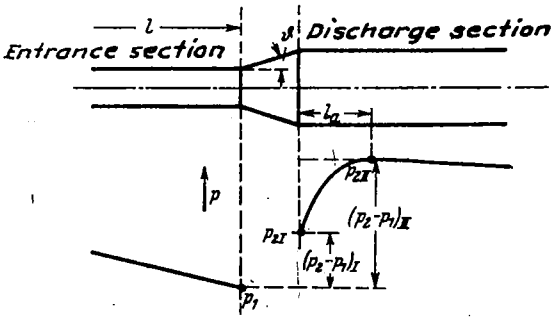

Figure 7. - Wall pressure in entrance and discharge length.

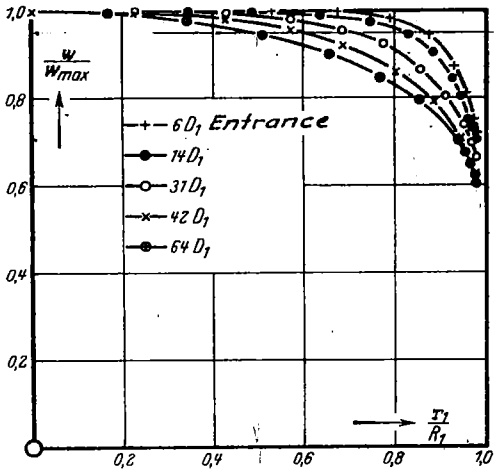

Figure 8. - Velocity distribution in entrance pipe with varying entrance (approach) lengths.

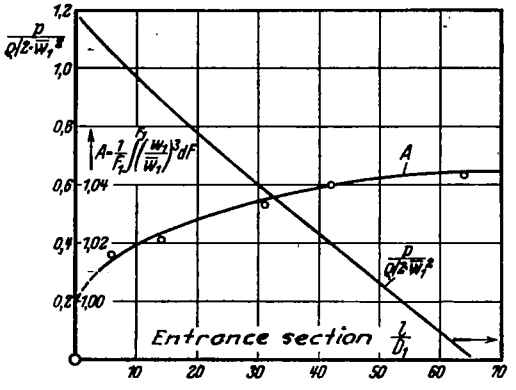

Figure 9. - Drop of pressure and flow of energy in entrance length.

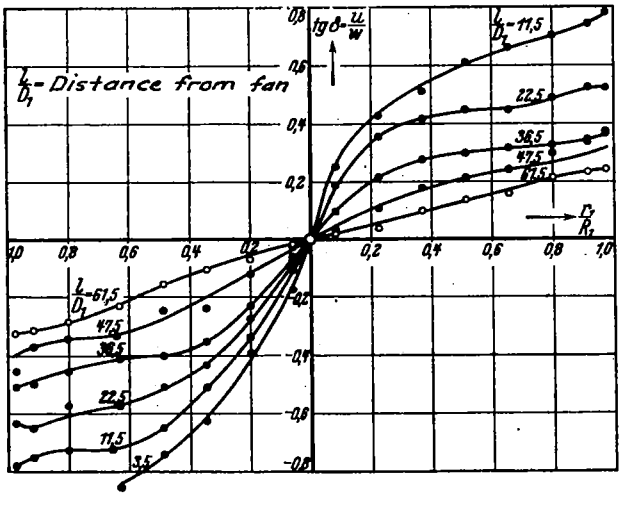

Figure 10. - Change of spiral flow with distance from spiral fan.

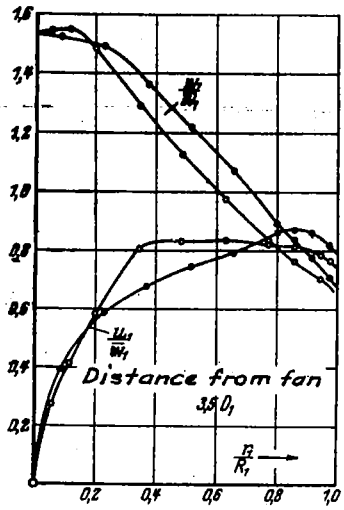

Figure 11.

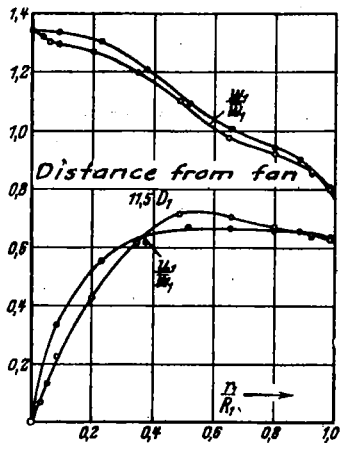

Figure 12.

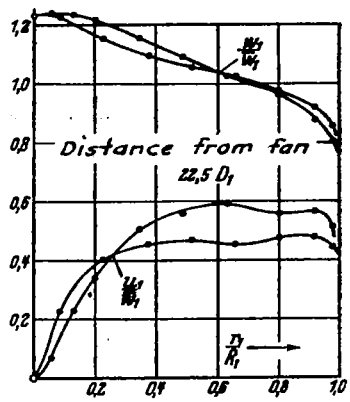

Figure 13.

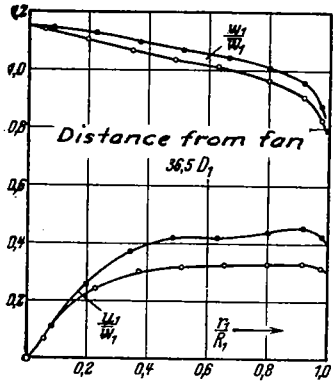

Figure 14.

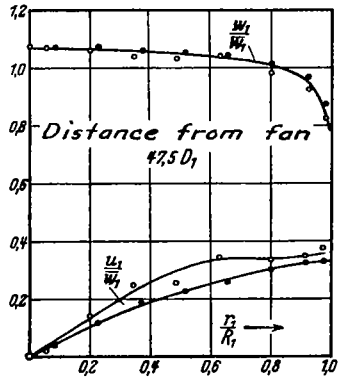

Figure 15.

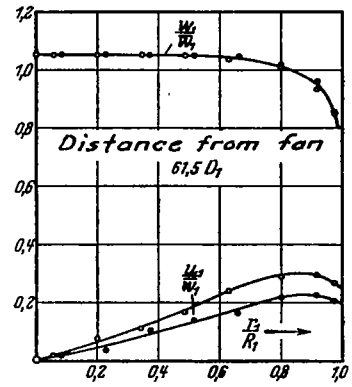

Figure 16.

Figures 11 to 16. - Velocity component of spiral flow.

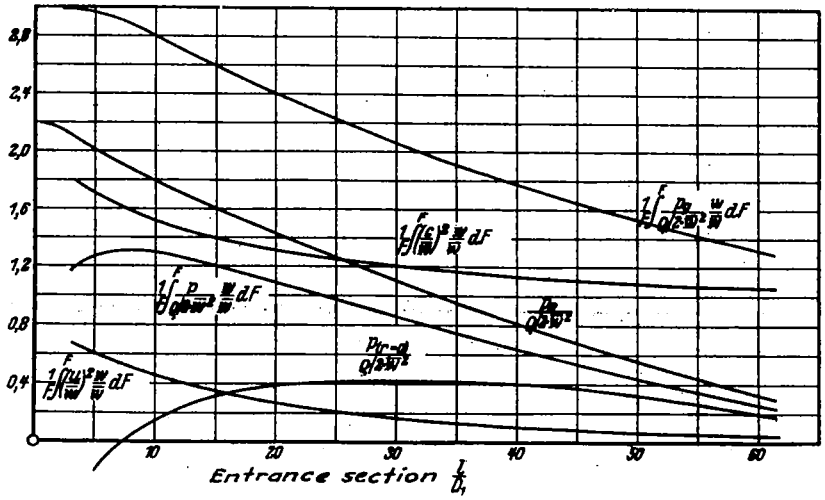

Figure 17. - Pressure and energy in entrance length with spiral flow.

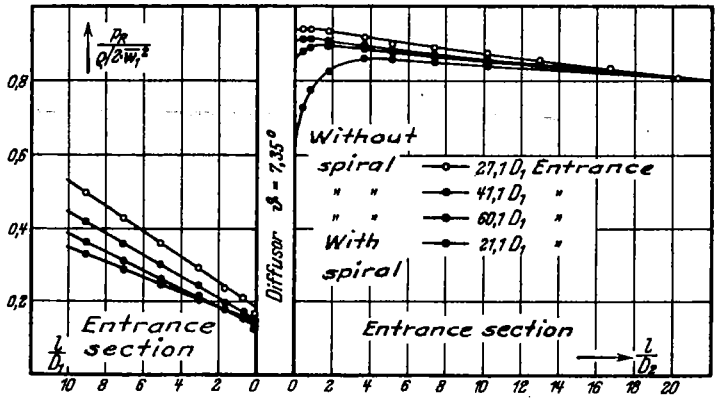

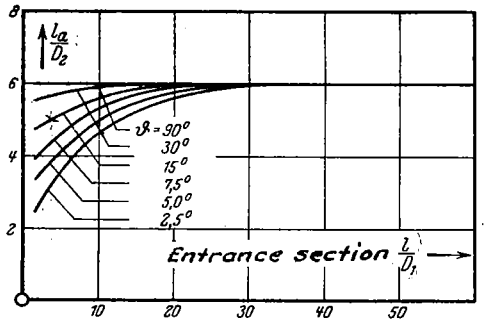

Figure 18. - Pressure at pipe wall in front of and behind the diffusor.

Figure 19. - Distance of pressure maximum from exit of diffusor.

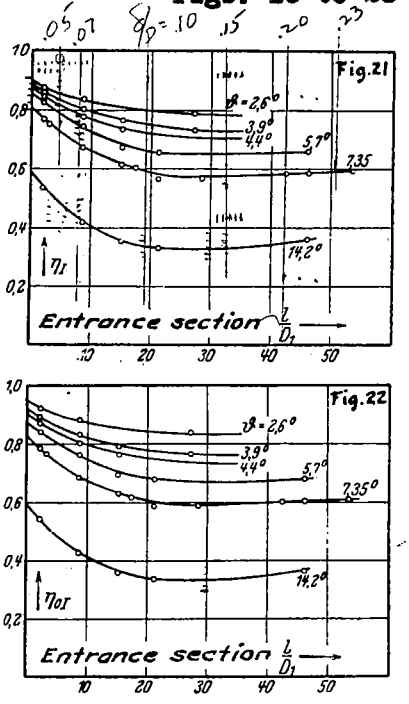

Figures 21 and 22. - Without discharge length.

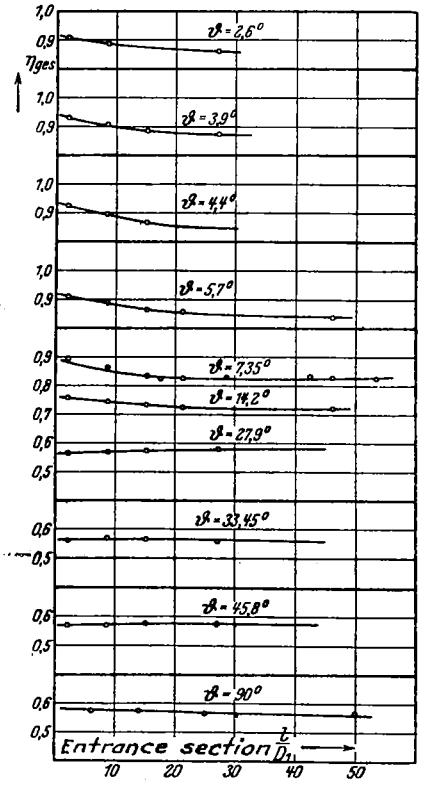

Fig. 20 Total efficiencies for diffusor with discharge length.

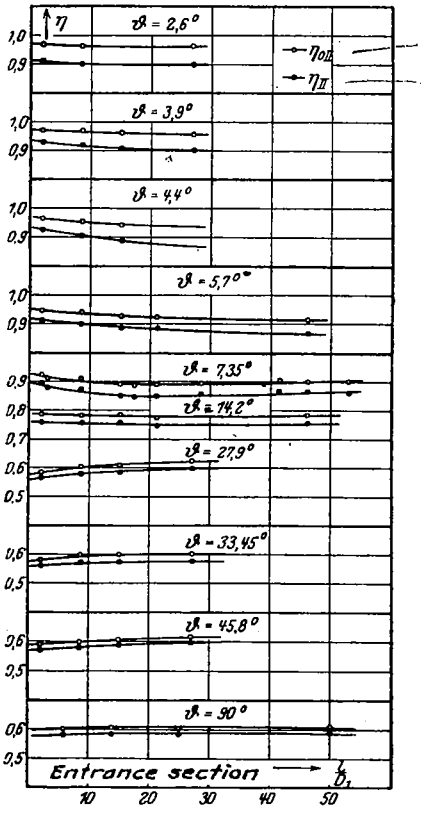

Figs. 21, 22, 23 - Efficiency of diffusor.

Figure 23. - With discharge length.

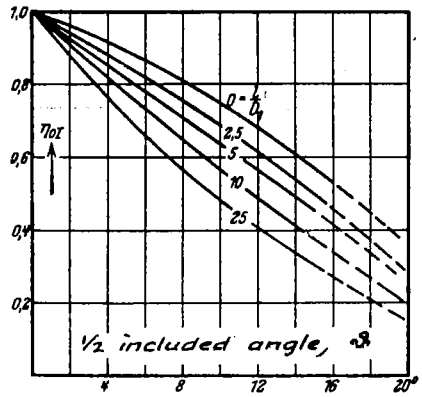

Figure 24. - Efficiency versus included angle of diffusor with different entrance lenghts.

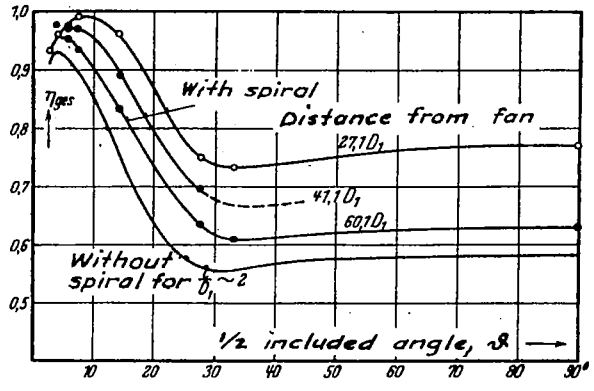

Figure 28. - Effect of spiral on efficiency.

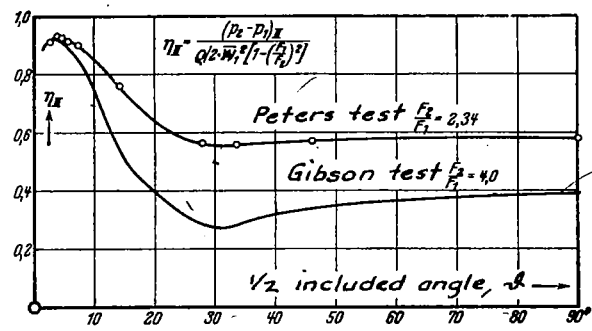

Figure 25. - Efficiency versus included angle for two ~~included angles~~ area ratios.

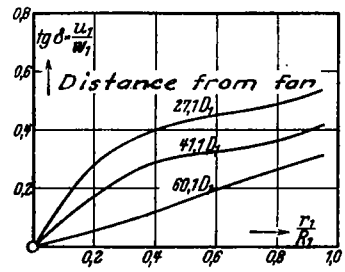

Figure 27. - Explored spiral flows.

$\frac{l}{d_1} = 2$

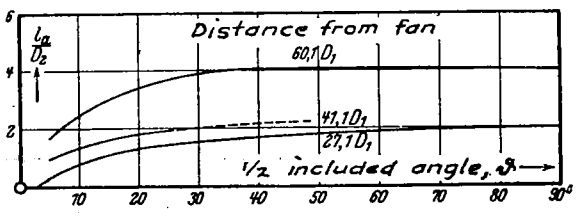

Figure 29. - Distance of pressure maximum from exit of diffusor with spiral flow.

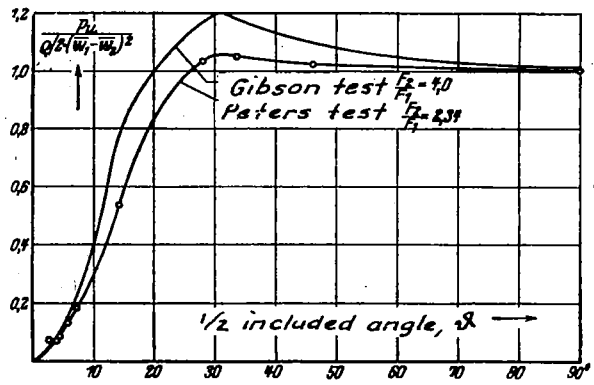

Figure 26. - Specific conversion loss.

page 1b